LIMITATIONS ON THE RESOLUTION OF YAG:CE BEAM PROFILE MONITOR FOR HIGH BRIGHTNESS ELECTRON BEAM

A. MUROKH, J. ROSENZWEIG

UCLA Department of Physics and Astronomy, Los Angeles CA 90095-1547, USA
E-mail: murokh@physics.ucla.edu

V. YAKIMENKO, E. JOHNSON, X.J. WANG

Brookhaven National Laboratory, Upton, NY 11973, USA
E-mail: yakimenko@bnl.gov

The performance of single crystal YAG:Ce ($Y_3Al_5O_{12}$) beam profile monitors was studied for transverse measurements on the high brightness ultrarelativistic electron beam at Accelerator Test Facility (ATF) at BNL. The test demonstrated systematic intensity dependent beam image enlargement on YAG monitors, compare to other diagnostics. Possible mechanisms of the effect have been studied. The quantitative examination was performed and compared to the developed phenomenological models. Limitations on the use of YAG:Ce diagnostics are discussed with respect to the high-brightness electron sources.

1 Introduction

YAG:Ce crystals (Yttrium Aluminum Garnet doped with Cerium) (Table 1) are widely used as a scintillators in electron microscopy (Fig. 1). Their excellent scintillating properties [1], vacuum-friendliness, mechanical rigidity and very long lifetime in a high radiation environment, made YAG:Ce an ideal candidate for diagnosing high brightness ultra-relativistic electron beams. There have been few very promising studies [2], which showed sub-micron resolution and excellent linearity of the beam-images taken with YAG:Ce crystal. Yet, there have been other indications showing image "blurring" at YAG:Ce beam profile monitors, as their performance was compared to the similar measurements with OTR [3, 4].

Table 1: Relevant properties of YAG:Ce crystal [5].

Index of Refraction	1.82
Wavelength of Peak Emission [nm]	525
Density [g/cm^3]	4.57
Radiation Length [cm]	3.6
Photon Yield [photons/MeV]	18 x 10^3
Scintillation Efficiency (compare to NaI)	45 %
Cerium Concentration (with respect to Y)	0.18 %

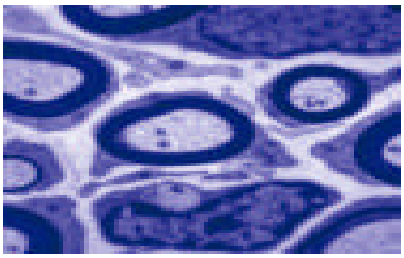


Figure 1: Photograph of a neuron, taken with electron microscope, using YAG:Ce.

As a part of VISA (Visible to Infrared SASE Amplifier) experiment [6, 7], (which requires intra-undulator measurements on a 1 nC beam with a RMS radius about 65 μm), we performed a study of YAG:Ce crystal applicability as a beam profile monitors at the ATF photo-injector facility [8,9]. Having focused the electron beam to small spot-sizes, we explicitly compared YAG:Ce performance to other diagnostics.

2 Experimental Set-up And Initial Results

An aluminum-base target was constructed with the two YAG:Ce crystals (0.50 mm and 0.25 mm thick respectively), a barium fluoride phosphor screen, and an OTR mirror (Fig. 2). In addition, a 20μm thin wire was stretched across the base gap for the x-ray wire scan measurements. The target was positioned on the motorized mount inside the Compton scattering beamline [10], allowing fast switching between the diagnostics.

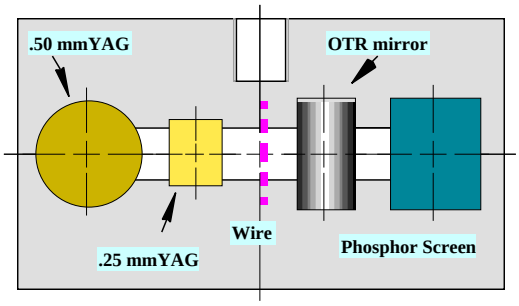


Figure 2: Motorized aluminum electron beam target equipped with 5 different diagnostics.

A single pulse photoelectron beam of 1 nC , with energy of 66 MeV, was focused on the target, and the radiation from the appropriate diagnostics was collected by the upstream parabolic mirror and imaged into the CCD camera. The resolution of the imaging system was measured to be better than 12 μm.

The first round of measurements demonstrated quite explicitly, that all the scintillating diagnostics produce much bigger image spot-sizes, than the ones measured with the OTR and wire-scan technique (Fig. 3). The difference in a FWHM of the beam measured with the different techniques was up to 200 μm, way above the resolution limits of the collecting optics. Without any assumption about the shape of the electron beam and background noise level, we can observe a significant size blurring on both YAG:Ce crystals, as well as on the phosphor screen (which was anticipated, due to the granular structure of the regular phosphorescent materials).

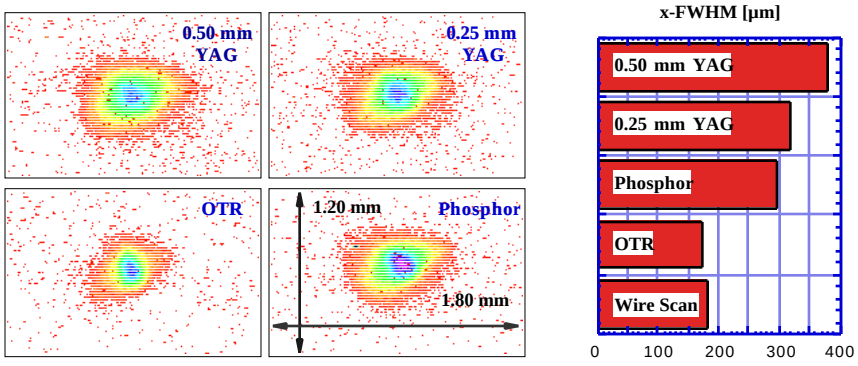


Figure 3: Beam spot images from YAG crystalls, compared to the OTR and standard phosphor. Also, full width half-maximum of a beam horizontal projection, for all four images, compared to the wire scan data.

Our first hypothesis concerning the poor YAG:Ce performance was related to the finite thickness of the crystal. The limitations on the imaging resolution associated with the finite thickness are indeed very specific to the crystal diagnostics. Unlike the OTR and phosphor diagnostics, where radiation "source" is allocated along a surface of negligible optical depth, YAG:Ce crystals radiate along the whole length of a particle path and at all the angles (as opposed to a well chosen Cherenkov radiator such as aerogel). Thus, one has to cut the acceptance of an imaging system to optimize the resolution and, yet, collect a fair amount of light (Fig. 4a). In addition over 20 % of the radiated light reflects from the back surface of the crystal, and for the finite emission angles further contribute to decrease in a transverse resolving power (Fig. 4b). In the most general case, we can write the approximate expression for the system optical resolution, as a function of crystal thickness, material index of refraction, and the angular acceptance in the optics:

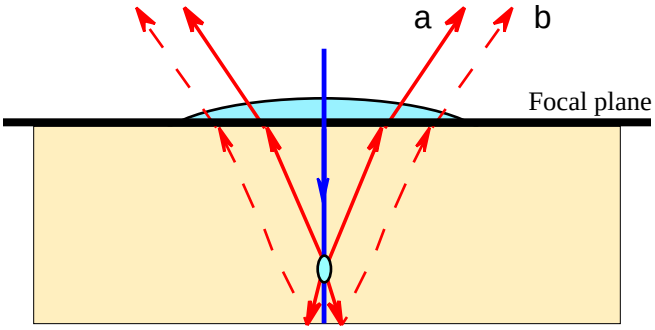


Figure 4: Limitations on YAG optical resolution at large emission angles. Image from a point source is not sharp due to: (a) finite crystal width, and associated depth of focus problem; (b) light reflection from the back wall of a crystal.

$$\sigma_f \approx \frac{d}{n} \tan\left(\frac{\theta_C}{2}\right) \qquad (1)$$

Our imaging system had an acceptance angle of 19° (to accommodate for the off-axis OTR light); and in the 500 μm thick crystal these effects increased an optical resolution from the telecentric limit of 12 μm up to 43 μm rms.

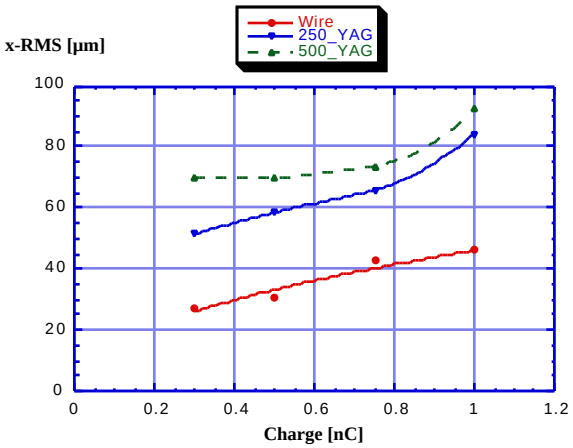


Figure 5: Charge dependence of the beam RMS size measured with different thickness YAG:Ce crystalls and a wire scan technique. The difference in measurements, between 250 μm and 500 μm thick YAGs can be described as an error of 35-40 μm added quadratically; unlike the difference with the wire scan measurements, which systematically increases for higher charge.

The difference in the performance of 250 and 500 μm YAG crystals (Fig. 5) can be fully attributed to the described depth of focus issue. Nevertheless, we were able to demonstrate, that overall it wasn't a dominant effect in the observed image 'blurring'. Positioning an aperture around the collimated beam (Fig. 6) dramatically improved the resolution, as it follows from (1); but did not remove a huge discrepancy between the YAG and OTR images.

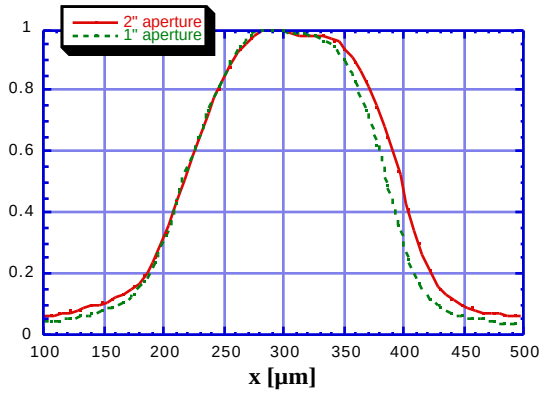


Figure 6: Beam profile measured with YAG:Ce crystal, for 19° and 10° acceptance angles of the imaging system. The difference in the measured beam width is 7 % only.

3 Discussion on Mechanisms of the Image Degradation in YAG:Ce

It is possible to distinguish two in principle different mechanisms, which would lead to the observed effects in YAG:Ce crystals: poor resolution associated with a *single electron behavior*, and the collective phenomena related to the *overall beam intensity*. Into the first category we include electron trajectory misplacements due to the scattering inside the YAG:Ce crystal; background noise from the x-rays and fast secondary electrons; optical impedance mismatch at the crystal surface and the depth of focus issues, discussed above. All the mentioned effects must have the same signature, regardless of the shape and intensity of the electron beam.

On the other hand, the beam intensity related effects associated with the total charge, or space charge field of the beam, must appear more significant for beams of the highest density or charge. Intensity related phenomena are more difficult to track as they may possess unique features under the different experimental conditions. Our data (Fig. 5) strongly suggest an intensity dependent nature of the image blurring, as the discrepancy in the beam spot-sizes measured with YAG:Ce and wire-scan technique increases for higher charge. Similar, intensity dependent

behavior was measured at APS [4]. Yet, in this section of the paper we will try to be systematic by reviewing a scintillating process in the YAG:Ce crystal and, at first, considering any single particle related effects, which can contribute to the observed beam image increase, well in excess of 50 μm RMS.

3.1 Review of the scintillating process

Properties of Ce doped single crystal scintillators have been thoroughly studied in the last decade, yet the complexity of the scintillation process results in rather phenomenological treatment [11]. It is generally viewed, that scintillation by the fast electrons in the inorganic scintillating materials is a 3-step process:

- electron-hole pairs (excitons) generation through the ionization processes by fast particles;
- excitons thermalization and transport from the host material towards the activator (in our case Ce^{3+});
- d-f level transitions, resulting in photon emission at the scintillating sites.

Single crystal YAG is an excellent host material, as it is transparent to the visible light, and the lowest d-f transition at the Ce site in YAG corresponds to 525 nm emission line.

Primary electrons, as they pass through the crystal, excite the valence electrons through Coulomb interactions, and kick them into the conductance band, producing holes. If the momentum transferred to the secondary electrons exceeds the minimum ionizing energy, they in turn produce more of free particles in collisions. Eventually, all the free charge carriers thermalize around the band gap energy (7 eV in YAG) and couple into the excitons (electron-hole pairs) [12].

Pair production is not a loss-free process. Energy transferred to the holes, as well as direct dissipation into heat, through emission of optical phonons, accounts for over a half of the energy deposited by the primary electrons [13]. There are number of models, developed to estimate the efficiency of pair production process [14], and simulations suggest, that in YAG:Ce about 60,000 e-h pairs are being produced, per MeV of energy transferred.

An exciton travels around the crystal, until the hole is trapped at the f-level of Ce ion (Fig. 7). Than, the emission takes place, peaked at around 525 nm. For the direct optical excitations of Ce ions at 480 nm, the quantum efficiency of the emission process was measured close to 100% [12]. In the case of excitation by the charged particles or γ-rays it is assumed to be ~ 100%; whereas, losses are generally being attributed to the non-radiative decay during the transport stage, when the excitons being trapped at the defect sites, or decay through the host emission [15]. For YAG:Ce single crystal, the industry standard for a photon yield is 17,000 photons/MeV [16], which means a useful emission by only one out of three e-h pairs produced.

3.2 Resolution of a Single Electron in YAG:Ce

There is some evidence [12] that the e-h pair can travel quite far inside the crystal (up to 40 μm, before the decay). That would put certain limits on the crystal resolution. However, the nature of such an effect is rather speculative; and we should use published experimental data on YAG:Ce resolution as a starting point.

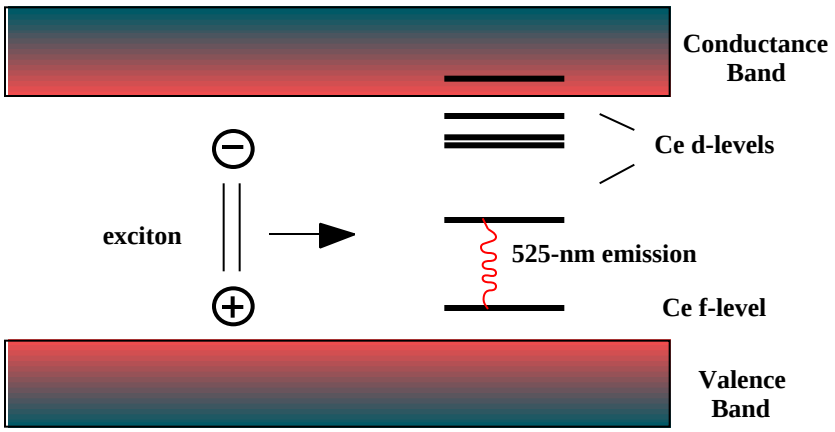


Figure 7: Schematics of the scitillation process in YAG:Ce. Thermalized electron-hole pair is being transported along the crystall and, eventually, trapped at the Ce-ion location. Trapped exciton is likely to decay through d-f transition, emitting visible light.

In the electron microscopy with YAG:Ce crystals (10-20 KeV electrons), resolution of few microns had been achieved. The measurements [17], that were performed at 2MeV (where the e-beam was masked with a knife-edge) demonstrated 30 μm resolution. In our case, we have 66 MeV electrons. Hence, the primary distinction from the above cases, is that our electrons can travel much further distances in the crystal, and produce more energetic secondary electrons, and bremsstrahlung x-rays.

3.2.1 Effects of Scattering on the Path of the Primary Particle

Let's consider a 0.5 mm thick YAG crystal. For the 66 MeV electrons projected RMS scattering angle in the crystal can be found $\theta = 20$ mrad. We are generally interested in the particles scattered at the angles larger than 100 mrad, for only those particles can directly contribute to the size "blurring" of more than 50μm. Clearly, for the multiple scattering 100 mrad is a far tail of the Gaussian distribution, which is negligible compare to the overall beam intensity. Single collisions at big angles would dominate the statistics [18], but their cross-section is still very small. The probability of such a collision is about 1 %:

$$n(\theta) \approx \frac{1}{\ln\left(204\ Z^{-1/3}\right)} \frac{\bar{\theta}^2}{\theta^2} \qquad n(100\ \text{mrad}) \approx 0.01 \qquad (2)$$

3.2.2 Penetrating X-rays and Secondary Electrons

Ultrarelativistic electrons interact with YAG crystal atoms, generating secondary particles, which can travel quite far inside the crystal. Again, in our case the travel distances of interest are limited to 50-100 μm in the plane perpendicular to the direction of motion. For the photons [19] it corresponds to the transverse momenta above 10 KeV, which are also very effective in activating scintillating sites [20]. Fortunately, the angular distribution of the bremsstrahlung photons has a narrow $1/\gamma$ cone in the direction of primary particle motion; hence, they can not be a source of noise far away from electron trajectory. Considering, that YAG is a crystal, there is a possibility of resonant Bragg diffraction [21] at the angles much larger than $1/\gamma$; however, taking into the account relative insensitivity of data to the crystal orientation angle, we should disregard this possibility.

In the case of secondary electrons, the required travel range corresponds to the particles faster than 100 KeV. Such energetic collisions have rather small cross-section and occur only to 1 out of 4 of incident particles, as they travel through 500 μm thick YAG crystal. Hence, we can conclude, that poor resolution in the crystal can not be due to the secondary particles.

3.3 Collective Effects by the e-Beam Electrons

The discussion from the previous section, let us believe, that the problem of image blurring is independent from any of the discussed effects. Also, from the less intense ultrarelativistic electron beams, the spot-sizes measured with YAG:Ce were reported as small as 11 μm RMS [2]. Hence, the key to the observed image degradation must be in the beam intensity dependent phenomena.

For the beams short compare to the YAG:Ce response time of about 80 ns [16], it is convenient to introduce a time-integrated current density Σ, as a measure of beam intensity:

$$\Sigma \equiv \int_0^{\tau} \vec{\mathbf{J}}(t)\ \hat{\mathbf{n}} dt \qquad \tau < 80\ \text{ns} \qquad (3)$$

In our measurements, the peak intensity Σ_p was up to 0.07 pC/μm^2. From [3] it follows, that the image blurring was observed at about Σ_p = 0.02 pC/μm^2, whereas the electron beam energy was 610 MeV.

3.3.1 Scintillating materials saturation for high beam densities

When the number of e-h pairs produced as a result of beam-crystal interaction, approaches the number of scintillating sites available along a path of the beam, the

saturation of an active medium may take place. Mathematically, the differential response of the medium to excitation can be formulated in the following way:

$$\frac{dn_{ph}}{dn_{eh}} = Q\beta\left(1 - \frac{n_{ph}}{QN}\right) \qquad (4)$$

where n_{eh} is a density of electron-hole pairs generated, and n_{ph} is the corresponding density of emitted photons; β and Q are transport and quantum efficiencies respectively, and N is a total density of Ce atoms.

The solution to the equation is straightforward, and can be written in terms of normalized variables:

$$R(x) = 1 - e^{-x}, \qquad \text{where } x \equiv \beta\frac{n_{eh}}{N}\ , R \equiv \frac{n_{ph}}{NQ} \qquad (5)$$

Thus, the normalized response is linear for the small x, and saturates exponentially as exciton density become comparable to the number of Ce sites available to emission process. In other words, as x approaches unity, one has to worry about the saturation.

The density of Ce ions, is a well-known parameter in the experiment. According to the Crytur Ltd., which supplied the crystal, $N \approx 2.5\ 10^{19}$ cm^{-3}. To find x we need to calculate the density of the e-h pairs generated in crystal:

$$n_{eh} \approx \frac{\Sigma}{e}\ 60{,}000\ \text{MeV}^{-1}\left(\frac{dE_i}{dz} + \frac{dE_{br}}{dz}\,\varepsilon(\gamma, d)\right). \qquad (6)$$

We have to consider separately bremsstrahlung and ionization energy losses by the primary electrons. The reason for that is, that only a fraction $\varepsilon(\gamma,d)$ of the bremsstrahlung radiation will be stopped inside the crystal, and it is generally dependent on the beam energy and the crystal thickness. More formal approach can be worked out; however, to simply check, if saturation can be an issue in our case, we can take the thick crystal limit (ε=1), and use the total energy loss ~ 20 MeV/cm, calculated for a 66 MeV beam and the material properties specified in Table 1.

As it was mentioned in *Section 3.1*, generally β is considered to be about 1/3 for a good quality YAG crystal, assuming the quantum efficiency of the emission Q is about unity. Yet, we find these assumption doubtful. It is only possible to measure experimentally the combined scintillation efficiency $\eta = \beta Q$, unless the emission is induced optically by the direct excitation of Ce f-d transitions. The experimental data demonstrate a non-trivial behavior even for optical excitations. The d-level of Ce is depleted into sublevels [22], due to the strong field in crystal, and the direct excitation spectrum for Ce has 4 peaks [12]. Yet, only the first excitation peak at 480 nm is intense, and the rest are weaker by at least a factor of three. Hence, it seems that the quantum efficiency of Ce luminescence actually depends on the excitation wavelength. By analogy, we may hypothesize, that in

the case of fast particle induced scintillation, Q depends on the energy of the trapped exciton, which is more likely to resemble shorter wavelength d-f excitations with higher probability of non-radiative quenching.

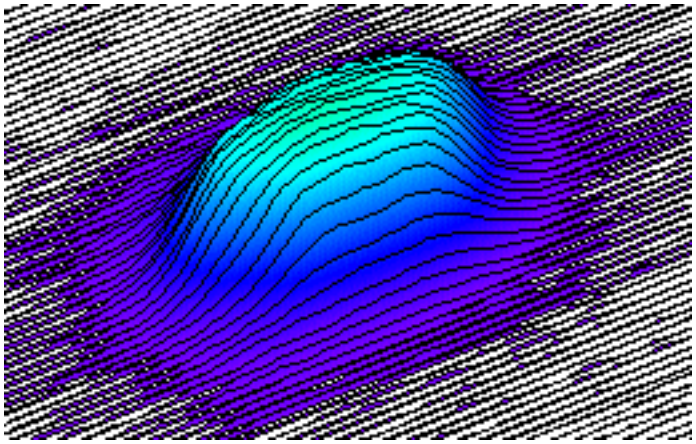


Figure 8: Flat-top shape of the YAG:Ce beam image is one feature that indicates saturation. All other diagnostics demonstrated sharply peaked profile.

More indirect evidence, that the QE differs from 100% in the case of scintillation by the fast particles follows from [16], where the photon yield was measured for YAG:Ce crystals with different concentration of Ce ions, varying from 0.05 to 1.08 %. If the losses were fully attributed to the transport stage, we would expect a significant improvement in the efficiency, as the Ce concentration increases, and transport length decreases. Yet the photon yield dependence on the Ce concentration was measured rather weak. Thus, we can conclude, that the data indicate more complex quenching mechanism than just a transport losses; and, therefore, β can be much closer to unity than the measured value of $\eta \approx 1/3$.

Again, we should take the extreme case of $\beta = 1$, and see if the YAG would saturate for our experimental conditions:

$$x_{\max} \approx \frac{\Sigma_p}{Ne} \; 60{,}000 \text{ Mev}^{-1} \; \frac{dE}{dz} \approx \frac{.07 \text{ pC } \mu\text{m}^{-2}}{4 \text{ pC } \mu\text{m}^{-3}} \; 120 \text{ mm}^{-1} = 2.1 \qquad (7)$$

Clearly, there is a strong saturation, which is typically responsible for the flat-top shape of the beam image (Fig. 8). To test the saturation theory with our data, we need to incorporate (5) into the beam shape measurements. If $\Sigma(r)$ describes the actual beam intensity profile, than we find the measured profile to be

$$\Sigma_m(r) = \frac{1 - e^{-\alpha \Sigma(r)}}{\alpha} \qquad (8)$$

The coefficient α has a straightforward physical meaning: the top limit on the beam intensity Σ that can be observed with YAG:Ce is α^{-1}. We can find the experimental value for α^{-1}, assuming, that the saturation is solely responsible for the image degradation in our data. One approach is to do the inversion of the expression (8):

$$\Sigma(r) = -\frac{1}{\alpha} \ln\left[1 - \alpha \Sigma_m(r) b\right] \qquad (9)$$

Since we don't know the relative scale for YAG and OTR data, it was necessary to include an additional parameter b into (7). Now we can perform a parametric fit, to match the inverted beam intensity from the YAG to the corresponding measurements with OTR (Fig. 9). By picking the most conservative set of we found, that α^{-1} does not exceed 0.01 pC/μm^2.

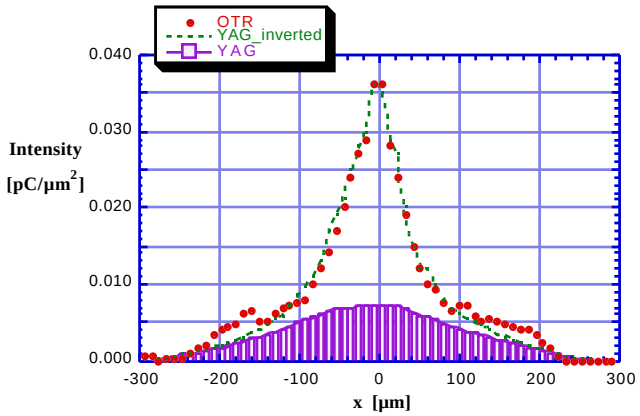


Figure 9: Saturation model for beam profile measured with YAG:Ce. The two parameters fit was performed to YAG data, to match inverted beam density with the OTR. As a result, the saturation parameter was found $\alpha^{-1} \sim 0.007$ pC/μm^2.

To test the formalism, the same procedure was attempted with the second set of data, where the YAG image of the higher density electron beam was compared to the wire scan measurements (Fig. 10). In general, it was more difficult to fit the data, and the resulting fit parameter α^{-1} was found twice bigger than in the case above, which indicates certain inconsistency.

In addition to quantitative disagreement between the two measurements, both values of α^{-1} do not obey the theoretical limit. From (4,5) we have already found a theoretical expression for α

$$\alpha = \frac{\beta}{eN}\ 60,000\ \text{MeV}^{-1}\left(\frac{dE_i}{dz} + \frac{dE_{br}}{dz}\varepsilon(\gamma,d)\right) \qquad (10)$$

In the worst case scenario, when all the assumptions favor saturation the most (namely, $\beta \approx \varepsilon \approx 1$), we obtain the bottom limit value for the saturation parameter $\alpha^{-1} = 0.033$ pC/μm^2, which is bigger than our experimental results.

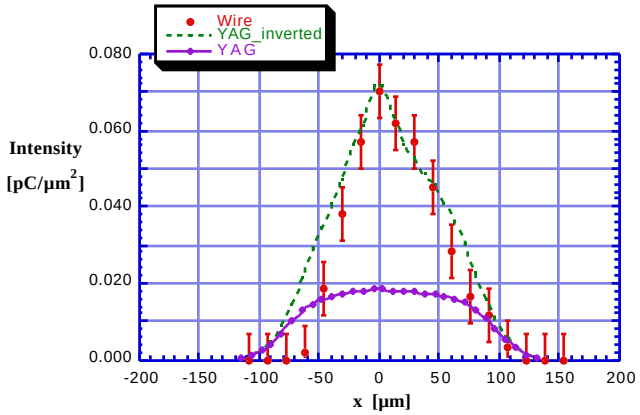


Figure 10: For the beam of higher density the fit parameter is found $\alpha^{-1} \sim 0.018$ pC/μm^2.

Despite the controversy, we believe, that this type of saturation is a real phenomenon reflected in our data. It also perfectly explains data presented in [3], where due to higher bremsstrahlung energy loss theoretical value for α^{-1} shifts down to the level of 0.01 pC/μm^2, and the reported discrepancy between YAG:Ce and OTR becomes significant around Σ_P = 0.02 pC/μm^2. Another example of saturation is observed in the comparison of γ-luminescence and α-luminescence [16]. When the α-particle passes through the crystal, it produces much denser ionization trace, than fast electron; which leads to a local "mini-saturation". As a result, the ratio of α/γ photon yield is about 0.5 for high efficiency crystals, and decreases for lower efficiencies. For YAG:Ce, this value is typically about 0.2.

Even though a model was developed, which demonstrated a YAG:Ce saturation possibility in our experimental condition; the quantitative agreement between our data and the theoretical analysis is far from conclusive. Therefore, we now look for additional causes of the image blurring.

3.3.2 Ionization Due to the Bulk Electric Field of the Beam

Another effect associated with the beam intensity is related to the space-charge field of the beam. The transverse force, exerted on the free electron by the Gaussian beam can be expressed as:

$$eE_r(t) = \frac{2eI(t)}{4\pi\varepsilon_0 c}\left[\frac{1-e^{-\frac{r^2}{2\sigma^2}}}{r}\right] \qquad (11)$$

It is easy to see, that for 1 nC beam with a peak current of 200 A, the space-charge field can be as high as 100 MV/m, depending on the actual transverse profile of the beam. This field is not quite strong enough to cause tunneling ionization in YAG:Ce; yet, it may enhance the avalanche ionization, seeded by the multiple scattering. Indeed, in such a field a free electron can accelerate to KeV energies within a picosecond, and as a result produce more electron-hole pairs.

The exact calculation of this effect is far beyond the scope of this paper. It is a cumbersome statistical problem, where the field does not dominate the dynamics of the slow electrons, and the field screening has to be taken into the account. We will use an oversimplified model, just to draw the general picture.

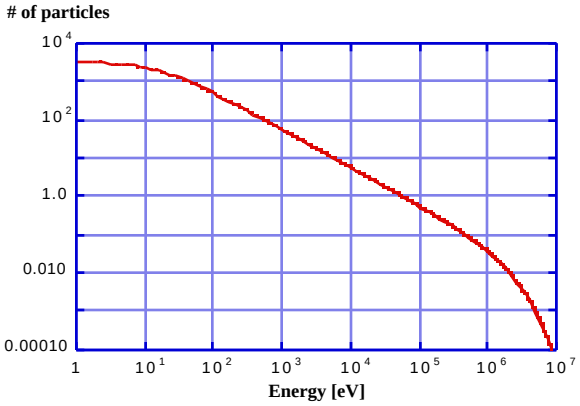


Figure 11: Energy spectrum of the secondary electrons, generated in 0.5 mm thick YAG, by a primary electron of energy 66 MeV.

First, let's look at the spectrum of the secondary particles (Fig. 11). About half of the energy lost by the primary particle is carried by the electrons with kinetic energy of few KeV or less. We can make a very rough assumption, that *the high energy half of the spectrum* is not affected by the beam space charge field at all. In

addition, we assume, that thermalization time of the *low energy half of spectrum* is negligible on the time scale of the beam. Indeed, the beam is few picoseconds long, compared to femtosecond thermalization time of sub-KeV electrons in plasma. Based on these simplifications, we can say that a half of the N thermalized conduction band electrons generated by the primary particle are generated instantly and will be affected by the space charge field of the beam.

These particles do not transfer momentum to valence electrons; therefore, they would accelerate by the field, till they reach ionization energy K_i ~10 eV. Then the accelerated particles produce more ions in collisions. We can calculate the time it takes for a particle initially at rest to gain energy K_i:

$$T(E) \approx \frac{\sqrt{2 m_e K_i}}{eE} \tag{12}$$

In the case of 100 Mev/m electric field, this time is $T(E)$ ~ 100 fsec. So, the ionized electron generated at the head of the beam, will "multiply" itself number of times, while the rest of the beam passes through the crystal. It should be noted that the distance that these multi-keV electrons travel is generally negligible on the scale of beam sizes of interest here. If no field screening is taken into the consideration, the total number of ionized particles increases by

$$G(E) \equiv \frac{N(E)}{N(0)} = \frac{1}{2}\left[1 + \frac{T(E)}{\tau \ln 2}\left(2^{\frac{\tau}{T(E)}} - 1\right)\right] \tag{13}$$

for $T(E) \le \tau$, where τ is an electron beam bunch length (in our case τ = 1.5 ps). It is convenient to introduce field value E_C such that $T(E_C) = \tau \ln 2$:

$$eE_C \equiv \frac{\sqrt{2 m_e K_i}}{\tau \ln 2} \approx 10 \text{ MeV/m} \tag{14}$$

With that formalism, we can directly write an expression for the ionization density yield:

$$n(r) \approx 3\ 10^4 \frac{\Sigma(r)}{e}\left[1 + \frac{E_C}{E(r)}\left(e^{\frac{E(r)}{E_C}} - 1\right)\right] \tag{15}$$

Of course, the exponential growth of ionization density must be limited by the field screening. This screening is due to charge separation in the nominally charge-neutral environment of the electron-ion system. Since the density of ion-electron pairs exceeds the electron beam density by orders of magnitude after only a short distance behind the beam head, this effect cannot be ignored (even though the charge separation distance is small compared to the beam size). We therefore can

expect some suppression of ionization gain. To account for this effect, we introduce the unknown screening coefficient ξ, , which takes values between zero and unity:

$$n(r,\xi) \approx 3\ \ 10^4 \frac{\Sigma(r)}{e}\left[1+\frac{E_C}{E(r)\xi}\left(e^{\frac{E(r)\xi}{E_C}}-1\right)\right] \qquad (16)$$

In this expression we assumed, that the value of ξ doesn't change along the beam profile, based on the fact that the field decay at the tails of the beam is inversely proportional to the distance from the center of the beam.

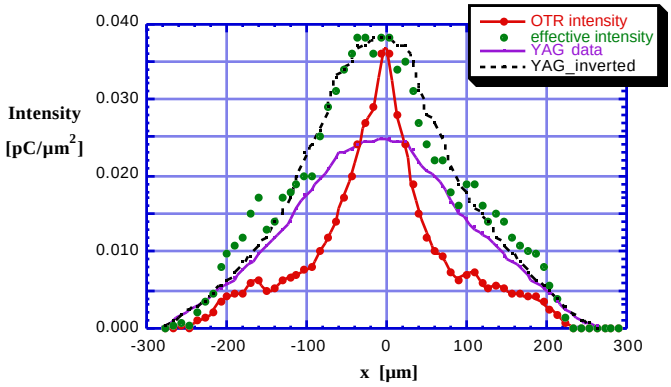


Figure 12: YAG:Ce beam profile measurements compared to OTR, using the saturation model with space charge enhanced ionization. "OTR intensity" represent the actual beam profile; "effective intensity" includes the ionization yield due to the space charge with the screening coefficient ξ = 0.42; "YAG data" curve represent the real YAG image, scaled in such a way, that the derived "YAG_inverted" makes the best fit to "effective intensity". Saturation coefficient, that provides for the best fit has a value $\alpha^{-1} \sim 0.04$ pC/μm^2.

Now, if we take into the account saturation, we can rewrite expression (8) for measured charge density, taking into the account field enhanced ionization:

$$\Sigma_m(r) = \frac{1}{\alpha}\left[1-\exp\left(-\frac{\alpha\Sigma(r)}{2}\left[1+\frac{E_C}{E(r)\xi}\left(\exp\left(\frac{E(r)\xi}{E_C}\right)-1\right)\right]\right)\right] \qquad (15)$$

Fitting this expression into the data (Fig. 12) is a two step process. First, one has to find an effective intensity (16), taking into the account the actual charge distribution measured with the OTR. To determine the unknown coefficient ξ it is

useful to look at the YAG image of the beam profile, and compare the fine features around the beam centroid to those of the effective intensity reconstructed for different screening coefficients. As difficult as it sounds, this procedure turned out to be an effective way to determine ξ quite accurately. Then we use the same inversion procedure (9) to determine the saturation coefficient α^{-1}, except the functional fit is being done to the effective density profile, rather than raw OTR data.

With this model, much better quantitative agreement has been achieved for different sets of data. Also, α^{-1} was found about 0.04 pC/μm^2, well within the theoretically predicted range.

4 Conclusion

We have experimentally established that the beam profile measured with YAG:Ce crystal can significantly differ from the beam as measured with other techniques. The nature of this effect is related to the beam intensity. First of all, it is possible to saturate scintillating sites in YAG:Ce crystal. Saturation becomes real at the beam intensities of the order ~ 0.04 pC/μm^2 for 100 MeV beam, and this limit scales with energy, inversely proportional to the beam energy loss function.

In addition to saturation, space charge ionization enhancement may contribute to the observed image blurring. According to our hypothesis slow electrons in the conduction band accelerate in the field of the beam, and produce additional ions in collisions. The effect becomes important for the high current beams focused down to ~ 100-200 μm spot-sizes. We believe that further experimental and analytical work is required to fully understand the problem and specify the exact combination of the mechanisms we have discussed. A new experiment would require an accurate calibration of photon collection diagnostics, in order to quantitatively establish the overall degree of saturation present in the YAG:Ce crystal.

Another related aspect of the future studies is search for the scintillators that do not saturate under high brightness beams. The crystals with larger band gaps (such as LuAG:Ce) or optically transparent crystalline ceramics can be considered.

Acknowledgements

The authors thank I. Pogorelsky and Compton group, for allowing to use their experimental set-up, and W. Graves, for helpful information, and stimulating discussions. The work was supported by the VISA collaboration, and done under DOE contracts No DE-AC02-98CH10886 and DE-FG03-92ER40693.

References

1. http://www.2spi.com/catalog/scintill/scintill.html
2. W. S. Graves *et al*., PAC 97 Proceedings, 1993-1995 (1998)
3. A. H. Lumpkin *et al*., Nucl. Instr. and Meth. A, **429**, 336-340 (1999)
4. Observations by ATF operators
5. http://www.crytur.cz/
6. http://www-ssrl.slac.stanford.edu/VISA/
7. A. Murokh *et al.*, FEL 99 Proceedings (1999)
8. X.J. Wang *et al*., PAC 99 Proceedings, 3495 (1999)
9. V. Yakimenko, same Proceedings
10. I.V. Pogorelsky *et al*., International Symposium on New Visions in Laser-Beam Interactions, Tokyo Metropolitan University, October 11-15, 1999
11. E. Zych *et al*., Spectrochimica Acta Part A **54**, 1771-1777 (1998)
12. E. Zych *et al*., Journal of Luminescence **75**, 193-203 (1997)
13. P.A. Rodnyi Radiation Measurements **29/4**, 235-242 (1998)
14. R.H. Bartram, A. Lempicki, Journal of Luminescence **68**, 225-240 (1996)
15. E. Zych *et al*., Journal of Luminescence **78**, 121-134 (1998)
16. T. Ludziejewski *et al*., Nucl. Instr. and Meth. A **398**, 287-294 (1997)
17. R. Nishi *et al*., Ultramicroscopy **63**, 273-278 (1996)
18. J.D. Jackson, *Classical Electrodynamics*, Second Edition, 650-651 (1975)
19. Particles Data Group (http://pdg.lbl.gov/)
20. M. Moszynski *et al*., Nucl. Instr. and Meth. A **404**, 287-294 (1998)
21. V.G. Baryshevsky, Nucl. Instr. and Meth. B **122**, 13-18 (1997)
22. H. Merenga *et al*., Radiation Measurements **24/4**, 343-346 (1995)